Influence of the Chemical Potential on the Hydrogen Sorption Kinetics of Mg_2Ni/TM/Pd (TM = transition metal) Trilayers

M. Pasturel,[†] R. J. Wijngaarden,[‡] W. Lohstroh,[§] H. Schreuders,[‡] M. Slaman,[‡] B. Dam,[‡] and R. Griessen*[,‡]

Unité Sciences Chimiques de Rennes, UMR CNRS 6226, Campus de Beaulieu bât. 10A, 35042 Rennes Cedex, France, Condensed Matter Physics, Department of Physics and Astronomy, Faculty of Sciences, Vrije Universiteit, De Boelelaan 1081, 1081HV Amsterdam, The Netherlands, and Forschungzentrum Karlsruhe GmbH, Institut für Nanotechnologie, Postfach 3640, 76021 Karlsruhe, Germany

Received September 11, 2006. Revised Manuscript Received November 29, 2006

The optical switching from shiny metallic to "black" absorbing states of 30 nm Mg_2Ni/50 nm TM/10 nm Pd (TM = Ti, V, Cr, Mn, Fe, Co, Ni, Pd) trilayer thin films upon hydrogenation is used to determine the hydrogen absorption/desorption kinetics at moderate H_2 pressure and room temperature. A strong correlation is observed between these kinetics and the enthalpies of solution of H in TM. A diffusion model based on chemical potentials of hydrogen in metals has been developed that agrees qualitatively with the experimental data, both from kinetics and hydrogen concentration profile points of view. The influences of the solution enthalpy and the diffusion coefficient of H in TM and that of the TM layer thickness are discussed with respect to this model. Finally, we conclude with potential applications of these trilayers, from optical hydrogen detection to reinvestigation of diffusion coefficients of H in TM.

1. Introduction

The societal acceptance of hydrogen as energy carrier in the coming years requires a high safety level and a continuous detection of hydrogen leaks. This implies the development of new generations of hydrogen sensors that have to be less expensive, safer, and more hydrogen specific than existing ones. Optical fiber hydrogen sensors are good candidates to fulfill these requirements.[1] Nevertheless, the sensing materials such as Pd,[2,3] WO_3,[4] V_2O_5,[5]... envisaged up to now present only small optical changes upon hydrogenation; complex techniques (Bragg grating spectroscopy,[6] microcantilever,[7]...) are needed to monitor the presence of H_2. Recently, metal hydride switchable mirrors[8] have been reported to exhibit drastic changes in reflection upon hydrogenation.[9−12]

For example, optical switching from shiny metallic to "black" absorbing with fast hydrogenation/dehydrogenation and cycling stability has been obtained for 30 nm Mg_2Ni/100 nm Ti/10 nm Pd trilayer thin films sputtered on glass.[11] Faster hydrogenation kinetics has been obtained on 30 nm Mg_2Ni or 50 nm $Mg_{70}Ti_{30}$/30−50 nm Pd bilayer thin films sputtered at the end of an optical fiber,[12] whereas preliminary studies on Mg_2Ni/Ni/Pd samples evidenced a remarkable asymmetry, i.e., fast hydrogenation and slow dehydrogenation rates.

To understand the origin of this intriguing behavior, we have systematically investigated the kinetics of hydrogenation/dehydrogenation for 30 nm Mg_2Ni/*x* nm TM/10 nm Pd (TM = Ti−Ni, Pd) trilayer thin films and reported the results in this paper. On the basis of calculations using a transfer matrix method and published dielectric functions for the individual layers,[13,14] all transition metals are suitable to obtain a large contrast in reflectance as a function of the hydrogen content in the Mg_2Ni layer. From a kinetic point of view, large differences are expected, because both hydrogen solubility and diffusivity vary by several orders of magnitude along the 3d transition metals.

A simple model taking into account the variation of the chemical potential of H in the constituting metallic layers is shown to qualitatively reproduce the main features of the experimental data. It is used to discuss the influence of (i)

* To whom correspondence should be addressed. E-mail: mathieu.pasturel@univ-rennes1.fr.
[†] Unité Sciences Chimiques de Rennes.
[‡] Vrije Universiteit.
[§] Institut für Nanotechnologie.

(1) Butler, M. A. *Appl. Phys. Lett.* **1984**, *45*, 1007.
(2) Butler, M. A. *Sens. Actuators, B* **1994**, *22*, 155.
(3) Villatoro, J.; Luna-Moreno, D.; Monzón-Hernández, D. *Sens. Actuators, B* **2005**, *110*, 23.
(4) Sekimoto, S.; Nakagawa, H.; Okazaki, S.; Fukuda, K.; Asakura, S.; Shigemori, T.; Takahashi, S. *Sens Actuators, B* **2000**, *66*, 142.
(5) Maciak, E.; Opilski, Z.; Urbanczyk, M. *J. Phys. IV* **2005**, *129*, 137.
(6) Sutapun, B.; Tabib-Azar, M.; Kazemi, A. *Sens. Actuators, B* **1999**, *60*, 27.
(7) Iannuzzi, D.; Deladi, S.; Slaman, M.; Rector, J. H.; Elwenspoek, M. C. *Sens. Actuators, B* **2006**, available on the Web May 19, 2006.
(8) Huiberts, J. N.; Griessen, R.; Rector, J. H.; Wijngaarden, R. J.; Dekker: J. P.; de Groot, D. G.; Koeman, N. J. *Nature* **1996**, *380*, 231.
(9) Pasturel, M.; Slaman, M.; Schreuders, H.; Dam, B.; Griessen, R.; Lohstroh, W.; Borgschulte, A. *J. Appl. Phys.* **2006**, *100*, 023515.
(10) Yoshimura, K.; Bao, S.; Yamada, Y.; Okada, M. *Vacuum* **2006**, *80*, 684.
(11) Pasturel, M.; Slaman, M.; Schreuders, H.; Borsa, D. M.; Dam, B.; Griessen, R. *Appl. Phys. Lett.* **2006**, *89*, 021913.
(12) Slaman, M.; Dam, B.; Pasturel, M.; Borsa, D. M.; Schreuders, H.; Rector, J. H.; Griessen, R. *Sens. Actuators, B* **2006**, available on the Web Oct 30, 2006.
(13) Lohstroh, W.; Westerwaal, R. J.; Noheda, B.; Enache, S.; Giebels, I. A. M. E.; Dam, B.; Griessen, R. *Phys. Rev. Lett.* **2004**, *93*, 197404.
(14) Lohstroh, W.; Westerwaal, R. J.; van Mechelen, J. L. M.; Chacon, C.; Johansson, E.; Dam, B.; Griessen, R. *Phys. Rev. B* **2004**, *70*, 165411.

10.1021/cm062157h CCC: $37.00
Published on Web 01/13/2007

the enthalpy of hydride formation or solution, (ii) the TM layer thickness, and (iii) the diffusion coefficient of hydrogen in the TM layer on the absorption and desorption kinetics. Finally, potential applications of such trilayer thin films are described.

2. Experimental Section

The 30 nm Mg_2Ni/*x* nm TM/10 nm Pd samples are prepared by dc magnetron sputtering (AJA ATC2400) from elemental sources in a vacuum chamber with an Ar base pressure of $\sim 1 \times 10^{-6}$ Pa. Mg and Ni are co-deposited on glass substrates with an atomic ratio of 2:1, checked by RBS analysis. The transition metal layer is then sputtered on top of the previous one. Subsequently, a 10 nm Pd cap layer is added in situ to protect the switchable mirror against oxidation and to promote hydrogen dissociation.

The thickness of the thin films is determined with a DekTak stylus profilometer.

Structural characterization is done in a Bruker D8 Discover X-ray diffractometer using Cu Kα radiation ($\lambda = 1.5418$ Å) and equipped with a 2D detector (Global Area Diffraction Detection System) that gives information about the orientation of the crystallites in the sample area diffracting the 0.5 mm diameter collimated X-ray beam. The sample is placed in a beryllium dome in order to measure diffraction patterns in various surroundings, namely air, H_2, or vacuum.

The optical reflection of the films is measured ex situ from the substrate side in an optical-fiber-based setup in the energy range $1.0 \leq \hbar\omega \leq 3.5$ eV (i.e., 1240 nm $\geq \lambda \geq$ 350 nm), with a 25° reflection angle. The setup allows Ar gas containing H_2 (0−100%) and/or O_2 (0−100%) to flow over the sample. The measured reflectances are calibrated with an aluminum reference mirror.

For electrochemical measurements in a galvanostatic mode, a constant current ($i = 13.3\ \mu A/cm^2$) is applied between the thin film ($\sim 1.5\ cm^2$) and a Pt counter electrode, whereas the potential is measured versus a Hg/HgO reference electrode. The electrolyte is 1 mol/L KOH flushed with 5N purity argon gas to remove dissolved gases. The cell is thermostated at $T = 293$ K. Variations of optical reflection and transmission during hydrogen loading and unloading are measured with a set of two diode detectors and a red diode laser with $\lambda = 635$ nm, i.e., $\hbar\omega = 1.95$ eV, mounted on the electrochemical cell.

3. Experimental Results

3.1. Kinetics of Hydrogen Absorption and Desorption. As mentioned above, trilayers of 30 nm Mg_2Ni/*x* nm TM/10 nm Pd are all expected to exhibit a transition from high to low reflectance, measured from the substrate side, upon hydrogen loading. So far, these theoretical expectations have been confirmed for TM = Pd and Ti.[11,12] Another example is shown in Figure 1 for TM = Fe and $x = 140$ nm. As expected, the as-sputtered reflection spectrum corresponds to that of Mg_2Ni.[14] The sample was then exposed to 5% H_2 in Ar, corresponding to 5 kPa partial pressure of H_2, and totally hydrogenates in about 120 s. The reflectance minimum in the hydrogenated state is due to destructive interference in the 30 nm transparent Mg_2NiH_4 layer covered with the reflecting transition metal layer. Upon exposure to 10% O_2 in Ar, the sample dehydrogenates; after 24 000 s for $x = 140$ nm and TM = Fe, the reflectance reverses to its initial value, implying a total release of hydrogen without noticeable deterioration of the thin film. Similar results are obtained for the other 3d-transition metals. The position of the reflectance minimum depends on the optical constants of the TM layer and occurs always in the 1.8−2.1 eV range, inducing a deep blue color of the samples observed from the substrate side.

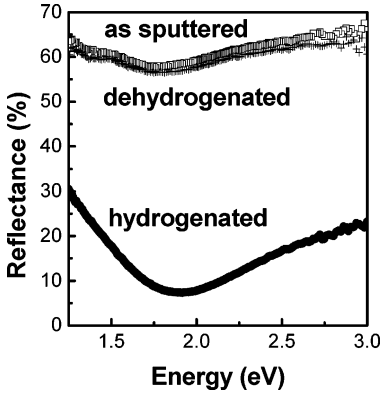

Figure 1. Optical reflectance spectra of a glass/30 nm Mg_2Ni/140 nm Fe/10 nm Pd trilayer film measured from the glass substrate side, in the (□) as-sputtered state, (●) hydrogenated state (120 s in a 250 mL min^{-1} flux of 5% H_2 in Ar) and (+) dehydrogenated state (24 000 s in a 250 mL min^{-1} flux of 10% O_2 in Ar).

The maximum optical contrast takes place in the red wavelength range. Therefore, the kinetics of hydrogen absorption and desorption are determined from reflectance measurements at 1.93 eV.

The time dependence of hydrogen absorption for a set of 30 nm Mg_2Ni/50 nm TM/10 nm Pd (TM = Ti, V, Cr, Mn, Co, Ni, and Pd) films is shown in Figure 2. The main features are as follows: (i) for TM = Co and Cr, the hydrogenation rates are slow (Figure 2a) and 48 h or 20 min are needed, respectively, to form the Mg_2Ni hydride (these two cases will be discussed in section 4.4); (ii) for TM = Ni, an almost linear decrease in the reflectance is observed from the unloaded to the fully hydrogenated state and takes place in about 60 s (Figure 2b); (iii) for TM = Pd and Mn, a straight and very fast hydrogenation is observed, the reflectance switching from above 50% to below 10% in about 10 s or less (Figure 2b); (iv) for TM = Ti and V, a fast partial decrease in the reflectance is observed initially but then the rate decreases progressively and the fully hydrogenated state is reached only after a few hours (Figure 2c).

The time dependence of hydrogen desorption for different 30 nm Mg_2Ni/50 nm TM/10 nm Pd (TM = Ti, V, Cr, Mn, Ni, and Pd) films is shown in Figure 3. Notice that data for the trilayer with TM = Co are not included, as after 9 months exposure to air, it was still not totally unloaded. The hydrogen release from TM = Ni samples takes place in a few hours (Figure 3a), as it does for TM = Fe. In the case of TM = Mn, approximately 30 min are needed to completely unload the samples. Finally, very fast desorption rates are observed for TM = Ti, V, and Pd (Figure 3b).

3.2. Electrochemical Hydrogenation/Dehydrogenation. To identify the various steps occurring during hydrogen absorption and desorption of the trilayer films, electrochemical loading and unloading has been performed in a galvanostatic mode (constant applied current). This technique, which involves large differences between the measured and equilibrium potential of the hydrides, is not appropriate for

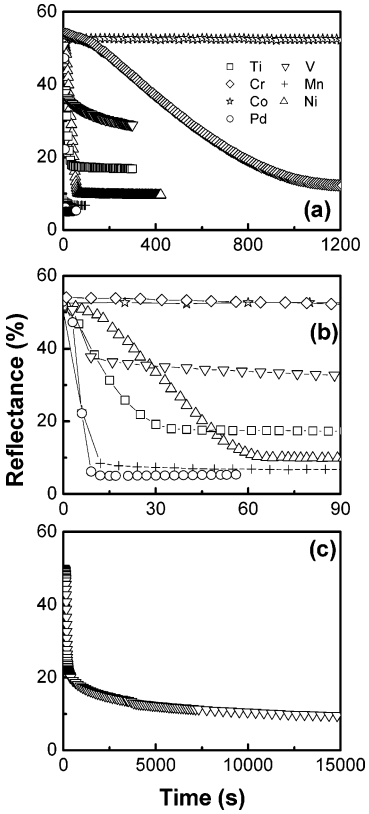

Figure 2. (a) Variation during hydrogenation of the reflectance at 1.93 eV of 30 nm Mg_2Ni/50 nm TM/10 nm Pd for TM = Ti (□), V (▽), Cr (◇), Mn (+), Co (☆), Ni (△), Pd (○) trilayer films exposed to a 250 mL min^{-1} flux of 5% H_2 in Ar; (b) zoomed area of (a) to highlight the behavior during the first 90 s; (c) enlarged time scale to show the total loading of the trilayer with TM = V.

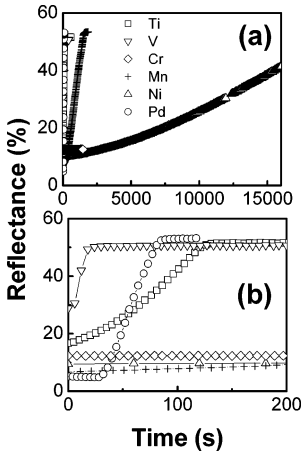

Figure 3. (a) Variation during dehydrogenation of the reflectance at 1.93 eV of 30 nm Mg_2NiH_4/50 nm TM/10 nm Pd (TM = Ti, V, Cr, Mn, Ni, Pd) trilayer films exposed to a 250 mL min^{-1} flux of 10% O_2 in Ar; (b) zoomed area of (a) to highlight the behavior during the first 200 s.

measurements of thermodynamic data. However, it is useful for comparison of the various reaction plateaus of different layers and the amount of H atoms exchanged that are proportional to the number of electrons Q. The results obtained on three typical 30 nm Mg_2Ni/50 nm TM/10 nm Pd trilayers are presented: (i) TM = Ni, in which the enthalpy of hydrogen solution is positive ($\Delta H_s \approx +12.5$ kJ/mol H)[15] (panels a and d of Figure 4), (ii) TM = Pd, in which the enthalpy of formation of α′-PdH_x ($-25 \leq \Delta H_f \leq -10$ kJ/mol H depending on H:Pd ratio)[16] is negative and higher than that of Mg_2Ni ($\Delta H_f = -31.7$ kJ/mol H)[13] (panels b and e of Figure 4), and (iii) TM = Ti with a hydride formation enthalpy ($\Delta H_f \approx -65$ kJ/mol H)[17] much more negative than that of Mg_2Ni (panels c and f of Figure 4).

For the trilayer with TM = Ni (Figure 4a), no plateau due to Ni is observed in the potential during hydrogen loading. This is in agreement with the high pressure of formation of NiH ($P_{H2} \approx 600$ MPa at 293 K),[15] whereas the stability of the electrolyte (1 M KOH) does not allow reactions below $E = -0.932$ V vs Hg/HgO, i.e., above approximately 1 bar hydrogen pressure. The relation between potentials and equivalent hydrogen pressures is described in ref 18.[18] Nevertheless, the sample turns into its black state, i.e., Mg_2NiH_4 is formed, after exchanging 5.8×10^{-7} mol(e^-)/cm^2. Considering the thickness of the Mg_2Ni layer (30 nm), its bulk density ($\rho = 3.43$ g/cm^3), its molecular weight (M = 107.2 g/mol), and an exchange of 1 electron per H atom, the maximum amount of electrons exchanged to form Mg_2NiH_4 is expected to be equal to $Q_{max} = 4 \times 1 \times ((30 \times 10^{-7} \times 3.43)/107.2) = 3.8 \times 10^{-7}$ mol(e^-)/cm^2. The experimental value is higher because at the potential of the reaction ($E < -1.2$ V vs Hg/HgO), both the hydrogenation of Mg_2Ni and the hydrolysis of electrolyte ($2H_2O + 2e^- \rightleftarrows H_2 + OH^-$) occur simultaneously. The same phenomenon is observed during the unloading (Figure 4d), where the optical reflectance increases slowly while the electrochemical potential saturates at the stability limit of the electrolyte ($1/2O_2 + H_2O + 2e^- \rightleftarrows 2OH^-$).

For TM = Pd (Figure 4b), a first plateau around $E = -0.9$ V vs Hg/HgO induces a strong decrease in the reflectance and a small increase in the transmittance. It is attributed to the formation of Mg_2NiH_4. A second plateau around $E = -1.0$ V vs Hg/HgO is then observed, accompanied by a small increase in the transmittance and no change in the reflectance. It is thus attributed to the formation of the palladium hydride. Further loading induces a decrease in the potential reaching that of electrolyte electrolysis, whereas no changes in *R* and *T* are observed. Such a loading behavior was expected from the formation enthalpies of the hydrides Mg_2NiH_4 and PdH_x ($0.6 < x < 1$): an H atom entering the thin film diffuses to the energetically favorable layer, i.e., Mg_2Ni layer (more negative ΔH_f) and then fills the second layer. According to this observation, the behavior during the unloading seems logical. The dehydrogenation first occurs in the PdH_x layer (plateau around $E = -0.55$ V vs Hg/HgO without changes in the reflectance and a small decrease in transmittance in Figure 4e) and then continues with the Mg_2NiH_4 layer (plateau around $E = 0$ V vs Hg/HgO with a concomitant important increase in the reflectance and a small decrease in transmittance in Figure 4e). Notice, the plateaus do not

(15) Wayman, M. L.; Weatherly, G. C. In *Phase Diagrams of Binary Hydrogen Alloys*; Manchester, F. D., Ed.; ASM International: Materials Park, OH, 2000; p 147.
(16) Manchester, F. D.; San-Martin, A.; Pitre, J. M. In *Phase Diagrams of Binary Hydrogen Alloys*; Manchester, F. D., Ed.; ASM International: Materials Park, OH, 2000; p 158.
(17) Manchester, F. D.; San-Martin, A. In *Phase Diagrams of Binary Hydrogen Alloys*; Manchester, F. D., Ed.; ASM International: Materials Park, OH, 2000; p 238.
(18) Cuevas, F.; Joubert, J.-M.; Latroche, M.; Percheron-Guégan, A. *Appl. Phys. A: Mater. Sci. Process.* **2001**, *72*, 225.

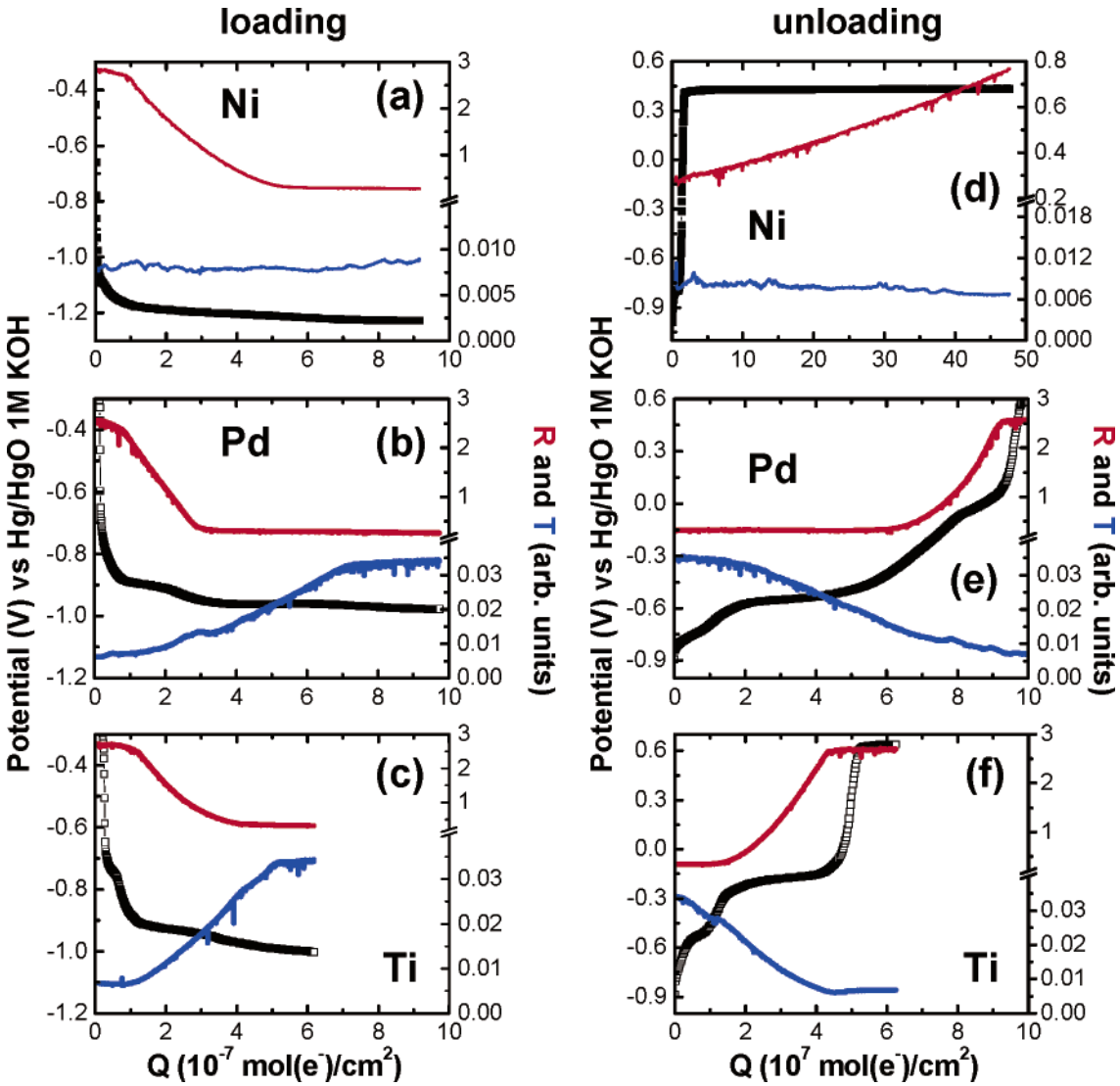

Figure 4. Variation of the electrochemical potential (vs Hg/HgO reference electrode) (black symbols), optical reflection (red line), and transmission (blue line) during galvanostatic (a−c) loading and (d−f) unloading of 30 nm Mg_2Ni/50 nm TM/10 nm Pd trilayer films with TM = Ni (a, d), Pd (b, e), and Ti (c, f).

respectively end and start sharply as expected, but the unloading of Mg_2NiH_4 seems to begin while the unloading of PdH_x is not yet completed. This will be discussed in section 4.2.

The same reasoning can be applied for thin films with TM = Ti. Panels c and f of Figure 4 represent the second loading and unloading of the sample, respectively. According to the highly negative enthalpy of formation of $TiH_{2-\delta}$ ($\Delta H_f \approx -65$ kJ/mol H),[17] electrochemical loading of the stack occurs first in the Ti layer (sloping plateau around $E = -0.7$ V vs Hg/HgO without changes in the reflectance and transmittance) and then in the Mg_2Ni layer (plateau around $E = -0.9$ V vs Hg/HgO with a strong decrease in reflectance and small increase in transmittance). The transmittance still increases slightly after the Mg_2Ni plateau, whereas the reflectance remains constant. This can be attributed to the loading of the 10 nm Pd top layer. The unloading first takes place in the Pd capping layer ($E = -0.55$ V vs Hg/HgO), and then in the Mg_2NiH_4 layer and finally in the $TiH_{2-\delta}$ layer (progressive increase of the potential toward the electrolyte electrolysis after the stabilization of reflectance and transmittance).

3.3. X-ray Diffraction. X-ray diffraction patterns obtained on 30 nm Mg_2Ni/50 nm TM/10 nm Pd trilayer films under different atmospheres are presented in Figures 5a−c for TM = Ni, Pd, and Ti, respectively. As-sputtered films exhibit a relatively sharp diffraction peak, namely Ni(111) at 44.50°, Pd(111) at 40.15°, and Ti(002) at 38.45°, indicating a clear oriented preferential growth of these layers during deposition. For TM = Ti and Ni, an additional peak corresponding to the Pd(111) top layer appears at 40.1°. No (003) or (006) peaks of the Mg_2Ni layer are observed at 20.1° or 40.9°, respectively,[14] because of (i) the relatively light weight of Mg, (ii) its position under the TM and Pd layers, and (iii) the very small size of the crystallites.[19] Each sample presents a different behavior upon exposure to hydrogen.

The Ni(111) peak observed at 44.50° in Figure 5a does not change in intensity and in position between the as-sputtered state and after exposure to 5 or 90 kPa H_2 pressure, in agreement with the very small solubility of hydrogen in

(19) Westerwaal, R. J.; Borgschulte, A.; Lohstroh, W.; Dam, B.; Griessen, R. *J. Alloys Compd.* **2005**, *404−406*, 481.

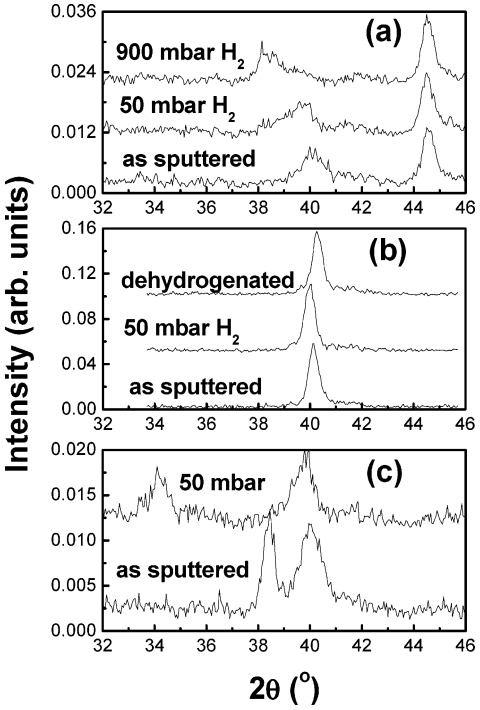

Figure 5. X-ray diffraction patterns of 30 nm Mg_2Ni/50 nm TM/10 nm Pd trilayer films with (a) TM = Ni, (b) TM = Pd, (c) TM = Ti under various gas atmospheres at room temperature. The curves are vertically shifted for clarity.

nickel ($\sim 3 \times 10^{-5}$ H/Ni)[15] at room temperature and moderate pressures.

The Pd(111) peak observed at 40.15° in Figure 5b is slightly shifted to smaller 2θ (40.00°) upon exposure to 5 kPa H_2 pressure, corresponding to the solution of hydrogen in the α-Pd phase. According to bulk thermodynamic data, α′-PdH_x forms at 293 K and $P(H_2) = 5$ kPa,[16] but this phase transition is observed only at higher pressure in the trilayer films (PdH_x(111) at 38.4° observed at $P(H_2) = 90$ kPa in Figure 5a). Strains within the trilayer films or size effects are known to influence the hydrogenation behavior of Pd[20−22] and thus the Pd layer. Samples exposed to primary vacuum are dehydrogenating and the peak is shifting to a slightly higher 2θ value than the initial one. Release of strains at the interface between Mg_2Ni and Pd layers can explain this observation.

Under 5 kPa H_2 pressure, the initial Ti(002) peak in Figure 5c disappears and the δ-$TiH_{2-\epsilon}$(111) peak appears at 34.3°. This hydride phase does not decompose upon exposure to primary vacuum or to air[23] because of its large negative enthalpy of formation, and only a small variation in the composition is observed ($0 < \epsilon < 0.4$).

The three series of experiments point toward a strong correlation between the hydrogenation behavior of the trilayer films and the enthalpy of hydrogen solution (or formation) of the transition metal layer. In the following section, this correlation is discussed with the help of a diffusion model based on the chemical potential of hydrogen in the system.

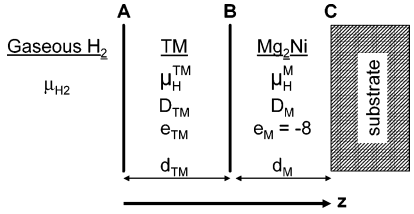

Figure 6. Schematic cross-sectional view of the bilayer thin film used to simulate the hydrogenation/dehydrogenation behavior. Each layer is characterized by its thickness d_X, its hydrogen diffusion constant D_X, and its reduced enthalpy of hydrogen solution (or formation) $e_X = (\epsilon_X - \mu^0_{H_2}/2)/RT$. The chemical potential of H in layer X is μ^X_H. It depends on the hydrogen concentration c_X, which is a function of space and time.

4. Discussion

4.1. Simulation of Diffusion. Several mathematical models have been developed to explain hydrogen diffusion through multilayer thin films.[24−27] Most of them use Henry's law to determine the hydrogen concentration in the metallic layer and define boundary conditions at the interface between two layers. Nevertheless, these models do not fit all the experimental data[28] or require different diffusion coefficients for identical layers.[25]

Here, another approach is proposed and a bilayer Mg_2Ni/TM on a substrate is considered. The transition metal layer (TM) has a thickness d_{TM} and the Mg_2Ni layer (M) has a thickness d_M (Figure 6). The substrate does not react with H.

The chemical potential of H in both layers is assumed to be of the form

$$\mu^X_H(c_X) = RT\ln\frac{c_X}{1-c_X} + \epsilon_X \qquad (1)$$

where c_X is the fraction of interstitial sites occupied by H atoms in the metal at energy ϵ_X, R is the ideal gas constant, and X stands for TM or M.

The chemical potential of molecular H_2, considered as an ideal gas at low pressure, is given by

$$\mu_{H_2} = \mu_{H_2}{}^0 + RT\ln\frac{P_{H_2}}{P^0} \qquad (2)$$

where $\mu^0_{H_2}$ is the chemical potential in the standard condition of pressure P^0 and temperature.

At equilibrium, the chemical potential of H atoms must be equal everywhere in the sample, i.e.

(20) Salomons, E. M.; Feenstra, R.; De Groot, D. G.; Rector, J. H.; Griessen, R. *J. Less-Common Met.* **1987**, *130*, 415.
(21) Züttel, A.; Nützenadel, Ch.; Schmid, G.; Emmenegger, Ch; Sudan, P.; Schlapbach, L. *Appl. Surf. Sci.* **2000**, *571*, 162−163.
(22) Eastman, J. A.; Thompson, L. J.; Kestel, B. J. *Phys. Rev. B* **1993**, *48*, 84.
(23) Results to be published.
(24) Ash, R.; Barrer, R. M.; Palmer, D. G. *Br. J. Appl. Phys.* **1965**, *16*, 873.
(25) Takano, N.; Murakami, Y.; Terasaki, F. *Scr. Metall. Mater.* **1995**, *32*, 401.
(26) Schmitz, G.; Kesten, Ph.; Kirchheim, R.; Yang, Q. M. *Phys. Rev. B* **1998**, *58*, 7333.
(27) Yamakawa, K.; Ege, M.; Hirscher, M.; Ludescher, B.; Kronmüller, H. *J. Alloys Compd.* **2005**, *393*, 5.
(28) Schmitz, G.; Yang, Q. M.; Kesten, Ph.; Geyer, U.; Hülsen, U. v.; Reimann, K.; Kirchheim, R. *Defect Diffus. Forum* **1997**, *945*, 143−147.

$$\frac{1}{2}\mu_{H_2} = \mu_H^{TM}(c_{TM}) = \mu_H^{M}(c_M) \quad (3)$$

In a nonequilibrium state, during diffusion, the boundary conditions are

$$\text{(i)}\ \frac{1}{2}\mu_{H_2}(A) = \mu_H^{TM}(A) \quad (4)$$

at the interface between gaseous H_2 and the TM layer (interface A in Figure 6) and

$$\text{(ii)}\ \mu_H^{TM}(B) = \mu_H^{M}(B) \quad (5)$$

at the interface between the TM and M layer (interface B in Figure 6).

In each layer, μ_H^X depends on position z and time t. At any time t, μ_H^X is a continuous function of z, but to conserve H atoms, its first derivative must satisfy the following boundary condition at interface B

$$L_{TM}\frac{d\mu_H^{TM}}{dz}|_B = L_M\frac{d\mu_H^{M}}{dz}|_B \quad (6)$$

as the current density of H particles is given by

$$j_H = -L_X\frac{d\mu_H^X}{dz} \quad (7)$$

where the coefficient L_X is given by

$$L_X = \frac{D_X c_X}{RT}(1 - c_X) \quad (8)$$

This expression ensures that (i) with a constant diffusion coefficient D_X in the limit of low hydrogen concentrations, eq 7 reduces to

$$j_H = -D_X\frac{dc_X}{dz} \quad (9)$$

because, from eq 1

$$\frac{d\mu_H^X}{dc_X} = \frac{RT}{c_X(1 - c_X)} \quad (10)$$

and (ii) it takes into account site blocking effects proportional to $(1 - c_X)$.

Comparing eqs 7 and 9, the boundary conditions 6 reduces to

$$D_{TM}\frac{dc_{TM}}{dz}|_B = D_M\frac{dc_M}{dz}|_B \quad (11)$$

Note, however, that at the same interface B, eqs 1 and 5 lead to

$$\ln\frac{c_{TM}}{1 - c_{TM}}|_B + \frac{\epsilon_{TM}}{RT} = \ln\frac{c_M}{1 - c_M}|_B + \frac{\epsilon_M}{RT} \quad (12)$$

This implies that the concentrations c_{TM} and c_M on both sides of interface B are not equal.

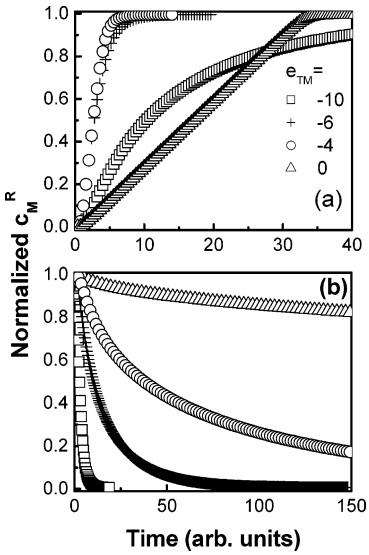

Figure 7. Simulated hydrogen (a) absorption and (b) desorption kinetics for 30 nm Mg_2Ni/50 nm TM bilayer films with different values of $e_{TM} = -10$ (□), -6 (+), -4 (○), 0 (△). The concentration c_M^R is the hydrogen concentration evaluated in the M layer at a distance of 3 nm from the M−substrate interface.

In the following, the dimensionless parameters $e_H = 1/2 \ln P_{H_2}/P^0$, $e_{TM} = (\epsilon_{TM} - \mu_{H_2}^0/2)/RT$, and $e_M = (\epsilon_M - \mu_{H_2}^0/2)/RT$ are used.

All simulations are done for $e_M = -8$, in agreement with the results of Lohstroh et al.[14] for Mg_2Ni thin films, which show that a homogeneous $Mg_2NiH_{4-\epsilon}$ layer can be obtained at $T = 293$ K and $P_{H_2} = 40$ Pa.

Finally, in the Mg_2Ni layer at the interface between M and the substrate (interface C in Figure 6), the particle current must vanish, because the substrate does not absorb H. Thus

$$\frac{dc_M}{dz}|_C = 0 \quad (13)$$

At each time of our numerical finite element method, two consecutive calculations are made:

- step 1: the diffusion equation

$$\frac{\partial c_X}{\partial t} = D_X\nabla^2 c_X \quad (14)$$

is solved for each layer X separately with appropriate boundary conditions $dc_X/dz|_{BorC} = 0$ and

- step 2: eq 12 is used on the pixel at position B in each layer with the constraint that the total H concentration on these two pixels is conserved, i.e.

$$c_{TM}^{old} + c_M^{old} = c_{TM} + c_M \quad (15)$$

where c_{TM}^{old} and c_M^{old} are the results from the diffusion eq 14. Equations 15 and 12 are a solvable set of two nonlinear equations with two unknowns c_{TM} and c_M.

The results are presented in the following sections.

4.2. Simulated Hydrogen Absorption and Desorption Kinetics. First, a 30 nm Mg_2Ni/50 nm TM bilayer is considered during H loading with $e_H = -2$ and unloading with $e_H = -13$. The time dependence of the concentration c_M^Revaluated at a distance of 3 nm from the Mg_2Ni/substrate interface is indicated in panels a and b of Figure 7for different

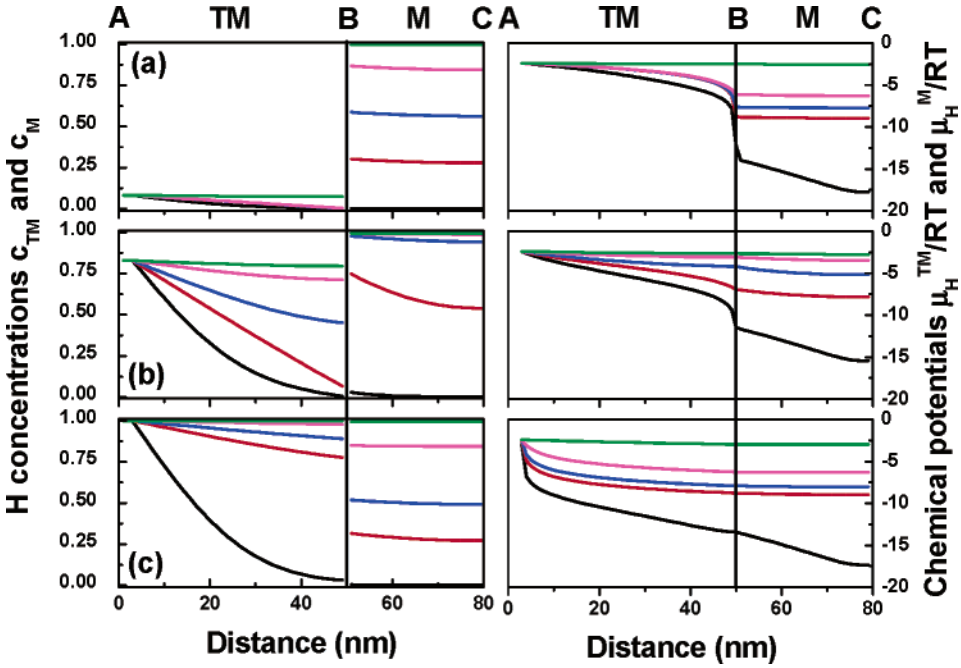

Figure 8. Simulated hydrogen concentration c_{TM} and c_M (left) and chemical potentials μ_H^{TM} and μ_H^M of hydrogen (right) profiles in 30 nm Mg_2Ni/50 nm TM bilayer films at 5 equidistant times (black < red < blue < pink < green) during hydrogen loading, for (a) $e_{TM} = 0$, (b) $e_{TM} = -4$, and (c) $e_{TM} = -10$. Notations of layers and interfaces are identical to those in Figure 6.

values of e_{TM}. This hydrogen concentration essentially determines the reflectance that is measured from the substrate side. It is thus meaningful to look for a correlation between the calculated concentration c_M^R and the measured reflectance in Figures 2 and 3. Note, however, that an increase in H concentration corresponds to a decrease in reflectance, because of the measured trilayer switch from shiny metallic to black absorbing during hydrogenation.

The calculations lead to the following conclusions:

(i) For $e_{TM} \geq 0$, c_M^Rincreases essentially linearly with time. This situation corresponds to TM = Fe or Ni that have positive enthalpies of hydrogen solution ($\Delta H_s \approx +27$ and +12.5 kJ/mol H, respectively).[15,29] This behavior is observed experimentally in Figure 2b for TM = Ni.

(ii) For $e_M < e_{TM} < 0$, the fastest hydrogenation rates are obtained. This configuration corresponds to TM = Pd or Mn ($\Delta H_s \approx -7$ kJ/mol H).[30] Experimentally, these transition metals also give the fastest hydrogenation rates, the samples being completely loaded within 10 s (Figure 2b).

(iii) For $e_{TM} < e_M$, c_M^R first increases rapidly but slowly decreases, and the fully loaded state is reached only after a relatively long time. Experimentally, such a behavior has been reported previously[11] for 30 nm Mg_2Ni/100 nm Ti/10 nm Pd films that reach a "black state" after 60 s but whose optical spectrum continues to evolve up to 210 s. It is also observed in Figure 2a−c for the 30 nm Mg_2Ni/50 nm V/10 nm Pd trilayer film. Both Ti and V (solution in the α-phase: $\Delta H_s \approx -31$ kJ/mol H or formation of the β_1-phase: $\Delta H_f \approx -41$ kJ/mol H)[31] have a more negative enthalpy of hydrogenation than Mg_2Ni.

The good qualitative agreement between experimental and simulated hydrogenation kinetics indicates that enthalpies of solution of hydrogen in the various layers play an essential role.

To gain more insight in the simulations, the concentration c_X and corresponding μ_H^X profiles are calculated in the bilayers at five equidistant times between the unloaded and fully loaded states and plotted in Figure 8a−c.

The boundaries conditions (eq 11−13) are fulfilled: (i) the chemical potential of H is continuous at the TM/Mg_2Ni interface, (ii) the slopes $dc_{TM}/dz|_B$ and $D_M\, dc_M/dz|_B$ are the same on both sides of interface B, and (iii) $dc_M/dz|_C = 0$ at the M−substrate interface.

For $e_{TM} = 0$ (Figure 8a), corresponding to TM = Ni or Fe, the Mg_2Ni layer can be totally filled ($c_M = 1$) with a hydrogen concentration c_{TM} remaining at a very low level in the TM layer, in agreement with reported results[15] and as observed during electrochemical loading (Figure 4a) or by X-ray diffraction (Figure 5a). In this case, a quasistationary linear gradient is rapidly established in the TM layer. This implies a constant current of particles through this layer and a filling of the M layer linearly in time (Figure 7a). The concentration c_M is always much larger than c_{TM} near the TM−M interface (B in Figure 6), because the enthalpy of hydride formation in M is more negative than that in TM.

For $e_M < e_{TM} < 0$ (Figure 8b), corresponding to TM = Mn or Pd, the Mg_2Ni layer is almost totally hydrogenated (red or blue lines), whereas the TM layer remains partially unloaded. It loads to its maximum value afterward, in agreement with the experimental electrochemical hydrogenation (Figure 4b). Notice that this maximum value is smaller

(29) Manchester, F. D.; San-Marin, A. In *Phase Diagrams of Binary Hydrogen Alloys*; Manchester, F. D., Ed.; ASM International: Materials Park, OH, 2000; p 46.

(30) San-Marin, A.; Manchester, F. D. In *Phase Diagrams of Binary Hydrogen Alloys*; Manchester, F. D., Ed.; ASM International: Materials Park, OH, 2000; p 95.

(31) Fagerstroem, C.-H.; Manchester, F. D.; Pitre, J. M. In *Phase Diagrams of Binary Hydrogen Alloys*; Manchester, F. D., Ed.; ASM International: Materials Park, OH, 2000; p 273.

than $c_{TM} = 1$. This agrees with the impossibility of forming PdH at moderate H_2 pressures.

In the opposite case for $e_{TM} < e_M$ (Figure 8c), corresponding to TM = Ti or V, the TM layer needs to be almost fully loaded before c_M starts to increase in the Mg_2Ni layer (red and blue lines). The same loading behavior is observed experimentally in Figure 4c.

Qualitative results of hydrogen absorption given by the diffusion model match the experimental results, from both the point of view of kinetics and that of hydrogen concentration profiles. For desorption, similar simulations are done (Figure 7b) starting with (i) hydrogen concentrations c_M and c_{TM} obtained in the fully loaded state by loading simulations and (ii) $e_H = -13$ corresponding to a negligible H_2 pressure, in order to compare them with the experimental dehydrogenation kinetics.

A huge increase in dehydrogenation time for a 30 nm Mg_2Ni/50 nm TM bilayer film is calculated (Figure 7b) when e_{TM} increases from −10 to 0. Experimentally, this agrees qualitatively with an unloading in a few seconds for TM = Ti and V (Figure 3b), in about 30 min for TM = Mn, and in a few hours for TM = Ni or Fe (Figure 3a). In these last two cases, the remarkable asymmetry between the fast hydrogen absorption and the slow desorption is confirmed by the simulations. Nevertheless, an exception occurs for TM = Pd, where the experimental hydrogen release takes place in about 1 min, whereas a behavior similar to that of TM = Mn is expected. This might be due to (i) a larger Pd surface in the case of a thick (50 + 10 nm) Pd layer than in the thin (10 nm) layer deposited on top of each TM film, which favors the surface reaction between H atoms and O_2 during dehydrogenation, or (ii) an additional activation energy barrier between the TM layer and the Pd-capping layer that is obviously not present for TM = Pd.[32]

Hydrogen concentration profiles during the hydrogen release (not shown here) also follow the different steps evidenced by electrochemical measurements during dehydrogenation (Figure 4d−f).

We conclude that the diffusion model well-reproduces the main features of hydrogen absorption/desorption in 30 nm Mg_2Ni/50 nm TM (/10 nm Pd) thin films. So, it is used in the next sections to study the influence of the transition metal layer thickness and of the diffusion coefficient of H in TM.

4.3. Influence of the TM Layer Thickness. Hydrogenation times are calculated for three different values of e_{TM} (−10, −4, 0) and for various thickness of the transition metal layer (20, 50, 100, 150, and 200 nm) in each case. These hydrogenation times are plotted versus the TM layer thickness in Figure 9a and are compared to the same graph with experimental data obtained on 30 nm Mg_2Ni/x nm TM/10 nm Pd, with TM = Ti, Pd, Ni (Figure 9b). Both graphs are comparable. Whatever the thickness, the smaller hydrogenation times are observed for $e_{TM} = -4$ and for TM = Pd; hydrogenation of $e_{TM} = 0$ and TM = Ni are somewhat longer, and finally, the longest hydrogenation time is observed for $e_{TM} = -10$ and TM = Ti. Moreover, the slope

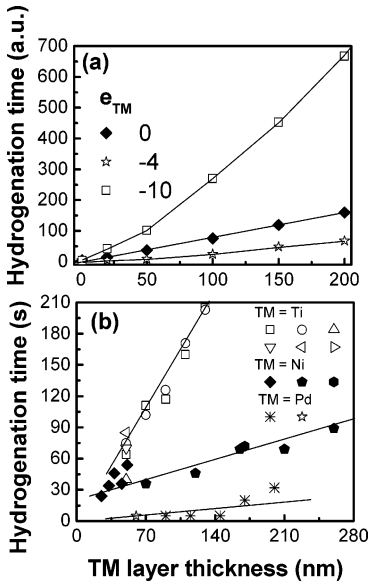

Figure 9. TM layer thickness dependence of the hydrogenation time of 30 nm Mg_2Ni/x nm TM (/10 nm Pd) thin films (a) simulated for $e_{TM} = -10$, −4, and 0 and (b) measured experimentally for TM = Ti, Pd, and Ni. Different symbols for a given TM in (b) correspond to samples from different batches.

of hydrogenation time versus TM layer thickness increases in the sequences $e_{TM} = -4 \rightarrow 0 \rightarrow -10$ and in the sequence TM = Pd → Ni → Ti. The model also qualitatively well-describes the influence of the TM layer thickness on the hydrogenation kinetics. Note that both calculated and experimental hydrogenation times increase more or less linearly with the TM layer thickness, whereas a quadratic dependence on the TM layer thickness would be expected in a simple diffusive system. It is a direct consequence of the difference in chemical potential between the Mg_2Ni and TM layers. Because of this difference, the gradient of hydrogen concentration in the transition metal layer is almost linear at any time *t*, except at the beginning (Figure 8). This implies that at a given time, the hydrogen concentration in TM at the interface B of Figure 6 decreases almost linearly with increasing thickness of TM. Or in other words, the time needed to reach a given c_{TM} at interface B increases almost linearly with the thickness of the TM layer. The equilibration of chemical potentials at the TM−Mg_2Ni interface (eq 12) induces a proportional increase in time to reach c_M in the Mg_2Ni layer, i.e., an almost linear increase of hydrogenation time with the TM layer thickness.

The same agreement between simulations and experiments is observed in Figure 10 for the dehydrogenation time dependence to the TM layer thickness, in the case of $e_{TM} = 0$ and −10 and the corresponding TM = Ti and Ni. In the case of $e_{TM} = -10$, a curvature is observed in the calculated dehydrogenation time versus TM layer thickness but is not in the experimental data. This difference could be explained by the surface reactions (PdH_x with O_2, intermediate formation of OH^-, release of H_2O formed) mentioned in section 4.2 that play an important role on the dehydrogenation kinetics.

4.4. Influence of the Diffusion cCoefficient of H in TM. Up to now, all the simulations have been done assuming the same diffusion coefficients of hydrogen in the M and

(32) Borgschulte, A.; Westerwaal, R. J.; Rector, J. H.; Schreuders, H.; Dam, B.; Griessen, R. *J. Catal.* **2006**, *239*, 263.

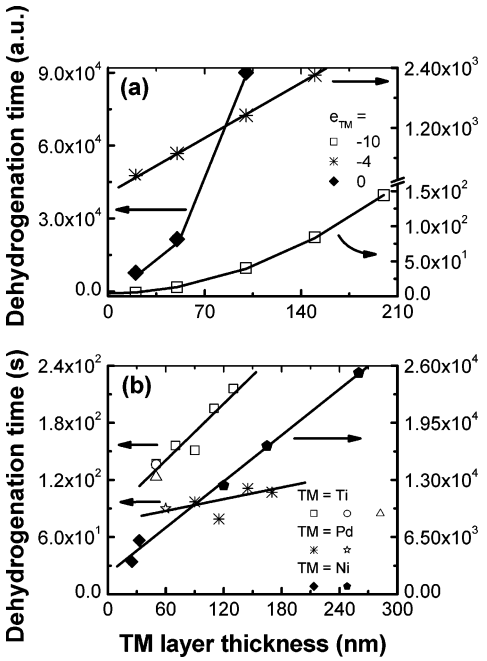

Figure 10. TM layer thickness dependence of the dehydrogenation time of 30 nm Mg_2Ni/x nm TM (/10 nm Pd) thin films (a) simulated for $e_{TM} = -10$, -4, and 0 and (b) measured experimentally for TM = Ti, Pd, and Ni. Different symbols for a given TM in (b) correspond to samples from different batches.

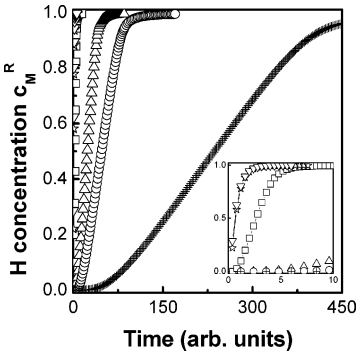

Figure 11. Simulated hydrogenation kinetics of 30 nm Mg_2Ni/50 nm TM ($e_{TM} = -4$) bilayer films for various ratios of diffusion coefficients of hydrogen in TM and M layers: $D_{TM}/D_M = 20$ (▽), 10 (☆), 1 (□), 0.1 (△), 0.05 (○), and 0.01 (+). The concentration c_M^R is the hydrogen concentration evaluated in the M layer at a distance of 3 nm from the M−substrate interface.

TM layers. Values reported for bulk transition metals,[33] however, show huge differences. Therefore, hydrogenation kinetics of 30 nm Mg_2Ni/50 nm TM (with $e_{TM} = -4$) bilayer films are simulated for different $D_{TM}/D_M = 20$, 10, 1, 0.1, 0.05, 0.01. The results are given in Figure 11.

For $D_{TM} > D_M$, a fastest hydrogenation is calculated in comparison with $D_{TM} = D_M$. Nevertheless, the hydrogenation time reaches a minimum limit (insert in Figure 11) that is probably determined by the diffusion of hydrogen in the M layer.

For $D_{TM} < D_M$, the hydrogenation times are inversely proportional to the value of D_{TM}: the hydrogenation time is 100 times longer for a 100 times smaller D_{TM}.

These simulations would imply strong differences in loading times of 30 nm Mg_2Ni/50 nm TM/10 nm Pd, between TM = V ($D_V \approx 1.2 \times 10^{-5}$ to 5.2×10^{-5} cm^2/s)[33,34] and TM = Ti ($D_{TiH_{2-\epsilon}} \approx 1 \times 10^{-17}$ to 9×10^{-13} cm^2/s)[35,36] or between TM = Fe ($D_{Fe} \approx 1.2 \times 10^{-5}$ cm^2/s)[33] and TM = Ni ($D_{Ni} \approx 1.4 \times 10^{-10}$ to 2.1×10^{-8} cm^2/s).[33,37,38] Experiments do not show such differences, with the loading time being very close in each case. Increased diffusion coefficients of hydrogen in both TM and Mg_2Ni layers due to a high concentration of grain boundaries can explain the difference between thin films and bulk compounds.[37−40] The texture of the transition metal layer, where a preferential growth of compact planes has been evidenced by X-ray diffraction, can also play a role if the hydrogen diffusion is not isotropic in TM.[41]

According to the enthalpy of solution of hydrogen in Cr ($\Delta H_s \approx +25.4$ kJ/mol H)[42] and in Co ($\Delta H_s \approx +20.9$ kJ/mol H),[43] hydrogen absorption and desorption kinetics of trilayer thin films are expected to be comparable with those of Ni and Fe, although they are experimentally much slower (Figure 2a). In these two examples, the diffusion coefficients of H in TM might play a role in slowing down the hydrogen absorption and desorption.

In all the simulations presented so far, the diffusion coefficients D_{TM} and D_M have been assumed to be invariant whatever the hydrogen concentration in the layers, as stated in section 4.1. This is close to reality for low hydrogen concentrations in the metal, e.g., Fe and Ni, but also for Pd at such low pressure. Nevertheless, in the case of Ti, V, and Mg_2Ni, an increase in c_H might induce a decrease in D_H. Such an influence, if known quantitatively, could be easily taken into account in our model.

4.5. Potential Applications. The diffusion model based on the chemical potential of hydrogen in metals enables us to qualitatively predict the hydrogen absorption/desorption behavior of a bilayer thin film including a metal hydride switchable mirror and a transition metal layer. It is thus valuable for the design of bi- or trilayer films with specific properties.

For an optical fiber hydrogen sensor, the fastest kinetics of hydrogenation is required and Mn and Pd are the most promising TM layer. This last element will be more suitable, according to the faster dehydrogenation kinetics, in the case of a thick Pd layer. Opposite, TM = Ni or Fe can be used

(33) Völkl, J.; Alefeld, G. In *Hydrogen in Metals I, Topics in Applied Physics*; Alefeld, G., Völkl, J., Eds.; Springer-Verlag: Heidelberg, Germany, 1978; Vol. 28, p 321.
(34) Remhof, A.; van der Molen, S. J.; Antosik, A.; Dobrowolska, A.; Koeman, N. J.; Griessen, R. *Phys. Rev. B* **2002**, *66*, 020101.
(35) Kaess, U.; Majer, G.; Stoll, M.; Peterson, D. T.; Barnes, R. G. *J. Alloys Compd.* **1997**, *259*, 74.
(36) Wipf, H.; Kappesser, B.; Werner, R. *J. Alloys Compd.* **2000**, *310*, 190.
(37) Palumbo, G.; Doyle, D. M.; El-Sherik, A. M.; Erb, U.; Aust, K. T. *Scr. Metall. Mater.* **1991**, *25*, 679.
(38) Brass, A. M.; Chanfreau, A. *Acta Mater.* **1996**, *44*, 3823.
(39) Tsuru, T.; Latanision, R. M. *Scr. Metall.* **1982**, *16*, 575.
(40) Abdul-Hamid, O. S. *Diffusion of Hydrogen in Titanium*. Ph.D. Thesis. Massachusetts Institute of Technology, Cambridge, MA, 1993.
(41) Cao, Y.; Li, H.; Szpunar, J. A.; Shmayda, W. T. *Mater. Sci. Forum* **2002**, *1139*, 408−412.
(42) Venkatraman, M.; Neumann, J. P. In *Phase Diagrams of Binary Hydrogen Alloys*; Manchester, F. D., Ed.; ASM International: Materials Park, OH, 2000; p 37.
(43) Griessen, R.; Riesterer, T. In *Topics in Applied Physics, Hydrogen in Metals II*; Alefeld, G., Völkl, J., Eds.; Springer-Verlag: Heidelberg, Germany, 1978; Vol. 29, p 73.

to keep the memory of an H_2 presence for a few hours without recording devices.

It should be mentioned that for application purposes, a good cyclability must be achieved without deterioration of the optical contrast and the kinetics of hydrogen sorption. Recent works reported a stability of these parameters during a high number of cycles on different systems: at least 20 cycles on Mg_2Ni/Ti/Pd films,[11] 50 cycles on $Mg_{70}Ti_{30}$/Pd films,[12] and even 450 cycles on Mg_4Ni/Ti-buffer/Pd trilayers.[44]

Nevertheless, a more complete model taking into account (i) the 10 nm catalytic Pd layer, (ii) the influence of surface reactions on the kinetics,[32] (iii) more precise values of enthalpies of solution of hydrogen in the nanostructured metal layers corrected for the strains in the thin films, and (iv) the influence of hydrogen concentration on its diffusion coefficient are needed for improved quantitative simulations. The films could then also be used to optically determine the perpendicular diffusion coefficient of hydrogen in different transitions metals in a manner very similar to that used by Remhof et al. for lateral diffusion.[34]

Conclusion

Hydrogen absorption and desorption kinetics from 30 nm Mg_2Ni/50 nm TM/10 nm Pd (TM = Ti−Ni, Pd) trilayer thin films have been shown to be strongly correlated to the enthalpy of solution of hydrogen in the transition metal layer, with the higher hydrogenation rate being obtained for $\Delta H_f(Mg_2NiH_4) < \Delta H_s(TM) < 0$.

The different kinetics observed as well as hydrogen profiles in the sample are qualitatively explained using a diffusion model based on the chemical potential of hydrogen in the metallic layers.

This model can be useful for designing thin films with adapted properties, depending on the required applications of these optically switching devices.

Moreover, comparison of experiments and simulations lead to the conclusion that for some transition metals, the diffusion coefficients of H are different in thin films compared with reported values in bulk metals, probably due to high concentration of grain boundaries or textured materials. Improvement of the model might enable a quantitative comparison with experiments and thus an easy determination of these diffusion coefficients.

Acknowledgment. The authors acknowledge the Stichting voor Fundamenteel Onderzoek der Materie (FOM) and the Nederlandse Organisatie voor Wetenschappelijk Onderzoek (NWO) for financial support through the Advance Catalytic Technology for Sustainability (ACTS) program.

CM062157H

(44) Bao, S.; Yamada, Y.; Okada, M.; Yoshimura, K. *Jpn. J. Appl. Phys.* **2006**, *45*, L588.